Reprinted from JOURNAL OF THE ATMOSPHERIC SCIENCES, Vol. 45, No. 12, 15 June 1988
American Meteorological Society

Observational Evidence of a Saturated Gravity Wave Spectrum in the Troposphere and Lower Stratosphere

DAVID C. FRITTS AND TOSHITAKA TSUDA*

Geophysical Institute and Department of Physics, University of Alaska, Fairbanks, Alaska

TORU SATO, SHOICHIRO FUKAO AND SUSUMU KATO

Radio Atmospheric Science Center, Kyoto University, Uji, Kyoto, Japan

(Manuscript received 27 April 1987, in final form 10 December 1987)

ABSTRACT

Radial velocity and temperature data obtained at the MU Radar Observatory during October and November 1986 are used to examine the character of the motion spectrum in the troposphere and lower stratosphere. It is found that the spectrum is dominated by low-frequency gravity waves with an upward sense of propagation in the lower stratosphere and both upward and downward propagation in the troposphere. Vertical wavenumber spectra of velocity and temperature are used to examine the consistency of the motion spectrum with the saturated spectrum of gravity waves proposed by Smith et al. Results indicate excellent agreement of the observed and predicted velocity and temperature spectra in both amplitude and slope. Vertical wavenumber spectra in area-preserving form reveal a dominant vertical wavelength of ~2.5 km, systematic variations in energy density and the dominant vertical scale with time, and consistency between the temporal variations of velocity and temperature variance. Taken together, our results provide strong support both for the view that velocity and temperature fluctuations are due primarily to internal gravity waves and for the saturated spectrum theory and its imposed constraints on wave amplitudes and spectral shape.

1. Introduction

Recent theoretical and observational studies have emphasized the importance of gravity waves and their associated momentum and energy transports in the large-scale dynamics of the lower and middle atmosphere. Their effects include, among others, a substantial drag on the large-scale flow at mesospheric and lower thermospheric heights (Lindzen 1981; Holton 1982; Dunkerton 1982; Vincent and Reid 1983; Fritts 1984; Miyahara et al. 1986; Fritts and Vincent 1987; Reid and Vincent 1987), the turbulent diffusion of heat and atmospheric constituents in these regions (Schoeberl et al. 1983; Thomas et al. 1984; Fritts and Dunkerton 1985; Strobel et al. 1985, 1987; Garcia and Solomon 1985), a smaller, but dynamically significant, drag applied in the lower stratosphere (Palmer et al. 1986; Tanaka 1986), and ubiquitous velocity and temperature fluctuations throughout the atmosphere (Fukao et al. 1981; VanZandt 1982; Philbrick et al. 1983; Vincent 1984; Meek et al. 1985; Balsley and Garello 1985; Larsen et al. 1986; Vincent and Fritts 1987). Despite the obvious importance of gravity waves in large-scale dynamics, however, our understanding of the characteristics and variability of the gravity wave spectrum and of those processes responsible for its excitation and spectral evolution is meager at the present time. Yet it is clear that such an understanding is necessary if we are to anticipate and account for the effects of such motions in the lower and middle atmosphere.

While studies of individual wave motions provide insights into the gross effects of wave transports and dissipation on the large-scale flow and allow us to address some of the mechanisms thought to be responsible for wave field saturation (Hodges 1967; Lindzen 1981; Fritts 1984; Fritts and Rastogi 1985; Hines 1988; Dong and Yeh 1988), it is clear that we must also consider the effects of a broad spectrum of wave motions in order to apply this understanding to the atmosphere. Recognizing this, a number of authors have examined the character, amplitude, and variability of the atmospheric motion spectrum using a variety of data. Horizontal wavenumber spectra were obtained using aircraft data (Lilly et al. 1974; Nastrom and Gage 1985), frequency spectra were compiled using radar and balloon data (Mantis 1963; Balsley and Carter 1982; Vincent 1984; Balsley and Garello 1985; Larsen et al. 1986; Yamanaka and Tanaka 1985), and vertical wavenumber spectra were obtained using balloon, radar, and rocket techniques (Endlich et al. 1969; Mantis and Pe-

* Permanent affiliation: RASC, Kyoto University, Kyoto, Japan.

Corresponding author address: Dr. David C. Fritts, Geophysical Institute, University of Alaska, Fairbanks, Alaska 99775-0800.

pin 1971; Dewan et al. 1984; Smith et al. 1985, 1987; Fritts and Chou 1987).

The vertical wavenumber spectra, however, provide the simplest means of examining the amplitude and composition of the motion spectrum for several reasons. First, the frequency spectra of horizontal and vertical motions obtained with ground-based techniques may depart from the intrinsic frequency spectra obtained following the mean fluid motion (Scheffler and Liu 1985; Fritts and VanZandt 1987), causing inferences about processes or the relative amplitudes of vertical and horizontal motions based on intrinsic frequency to be in error. Second, the horizontal wavenumber spectra are simply related to the vertical wavenumber spectra only if the frequency and wavenumber dependence of the gravity wave spectrum is separable, leading to ambiguity if this is not the case. Finally, and most importantly, the vertical wavenumber is directly related to the intrinsic phase speed and the saturated amplitude of a wave motion, yielding information on wave amplitudes and propagation that is otherwise difficult to infer. Thus, we use vertical wavenumber spectra in this study of atmospheric gravity wave motions.

Our purpose in this study is to examine the consistency of the amplitude of the observed gravity wave spectrum with that implied by wave field saturation (Dewan and Good 1986; Smith et al. 1987), to test the consistency of the observed velocity and temperature spectra with the gravity wave dispersion relation, to determine the characteristic vertical scale of the motion spectrum in the troposphere and lower stratosphere, and to examine the evolution of the spectrum with height and its response to changes in atmospheric stability. To do this, we use a unique dataset composed of high vertical resolution profiles of radial wind and temperature collected at the MU Observatory in Shigaraki, Japan, during October and November 1986. This dataset and the mean atmospheric structure observed during the experiment are described in section 2. We display in section 3 the fluctuating components of the motion and temperature fields and examine their variability as well as the dominant wave scales, phase progression, and amplitudes. This suggests that the spectrum is composed, in large part, of low-frequency, meridionally propagating motions with vertical wavelengths of ~2 km and amplitudes corresponding to those required for linear convective or dynamical instability of the wave field (Fritts and Rastogi 1985). The consistency of the vertical wavenumber spectra of velocity and temperature with the gravity wave dispersion relation and with those spectra predicted by the saturation theory of Smith et al. (1987) as well as the variability of these spectra with time are examined in section 4. It is found that there is good correspondence between the velocity and temperature spectra, in terms of both the dominant vertical wavenumber and the relative spectral amplitudes. We present in section 5 the mean velocity and temperature spectra obtained in the troposphere and lower stratosphere. These results show the spectral amplitudes to scale with atmospheric stability approximately as predicted by saturation theory, and provide strong support for the view that such motions are indeed manifestations of internal gravity waves. Our conclusions are presented in section 6.

2. Data description and mean atmospheric structure

The velocity data used in this analysis of atmospheric gravity wave motions were obtained with two oblique beams of the MU radar (35°N, 136°E) aligned east and north at 20° from zenith. For a general description of the MU radar and its capabilities, the reader is referred to the papers by Kato et al. (1984) and Fukao et al. (1985a,b). Data were collected for ~16 hours per day (during nighttime only) from 1600 local time (LT) on 17 October to ~0800 LT on 25 October and continuously from ~2200 LT on 26 November to ~1100 LT on 29 November 1986. The data were obtained with a range resolution of 150 m and a time resolution of ~1 min for altitudes from 5–25 km. The radial velocities at each height were subsequently averaged for one hour to increase confidence in the velocity estimates, to extend the useful data above 20 km, and to reduce the contamination of the radial velocities by the vertical component of the motion field. The resulting velocities extend above 20 km and can be viewed, to a good approximation, as projections of the horizontal motions on the oblique beam directions.

Temperature data were collected with a high-resolution balloon sounding system providing temperature and pressure information at ~5 s and 30 m height intervals. The resulting temperature profiles were smoothed with a 5-point running mean, yielding a dataset with a vertical resolution comparable to that of the radar. The balloon height was determined hydrostatically from the temperature and pressure data. During the October radar campaign, balloon soundings were made at ~2100 and 0200 LT each night except for 23 October, at which times the balloon failed. Balloon soundings were made during the November campaign at three-hour intervals beginning at 2000 LT 26 November and ending at 0900 LT 29 November.

Because of the strong zonal jet, balloons were typically advected downstream ~50–100 km during their ascent to ~15 km. This would present problems in a conjunctive radar and balloon analysis of high-frequency wave activity for which horizontal scales and correlation lengths are small. Our interest in this study, however, is in the more energetic, low-frequency component of the wave spectrum, which will be seen to dominate the velocity and temperature profiles during our observations. This domination by low-frequency motions, together with a preferred meridional sense of propagation of this component of the wave spectrum, suggests that the measured velocity and temperature

fluctuations of such motions should remain correlated over large distances.

The resulting velocity and temperature data were used to define the mean atmospheric structure for the purposes of describing the gravity wave environment and determining the fluctuations attributed to wave motions. Because the radar data obtained during October did not yield a complete diurnal description of the motion field, however, it was not possible to remove all contributions for motions near or lower than the inertial frequency (a 20.9-h period) due to Doppler shifting. Thus, the radar data for October were averaged for each 16-h data collection interval and a 3-km smoothing was applied. The extent of this smoothing was chosen to be larger than the characteristic vertical scale of the wave spectrum so as not to bias estimates of the saturated spectral amplitude or the dominant vertical wavenumber.

A similar procedure was employed for the temperature data because of the limited number of profiles available for a definition of the mean structure. In addition, the first four profiles obtained during the October campaign were treated separately because of the distinct and vertically confined fluctuation in the mean structure occurring near 10 km during this interval. To preserve this feature, which we believe was not associated with the wave spectrum, the smoothing of the mean temperature profile was applied only above and below this height during this period.

For consistency in the analysis, the November mean temperature and velocity profiles were also obtained using a 3-km smoothing, despite the fact that there were in this case sufficient data to determine more accurate mean profiles without applying the vertical smoothing. As a test of the sensitivity of the results to this procedure, we compared the temperature and velocity spectra obtained for November with and without this smoothing and found only minor differences.

The mean profiles of eastward and northward radial velocity, u_r and v_r, temperature, T, and Brunt–Väisälä frequency squared (or static stability), N^2, for the October and November periods are shown in Figs. 1 and 2. Temperature and stability profiles computed for the final three days of the October observation period are sufficiently similar to those for November that they are not shown. The mean radial velocity profiles reveal a well-defined zonal jet structure centered near 12 km with maximum radial velocities of $\sim$20 and 24 m s^{-1}, respectively, implying horizontal flow speeds of $\sim$60–70 m s^{-1}. In both data periods, the vertical extent of the jet corresponds closely to the region of transition between the less stable troposphere and the more stable stratosphere. Although not revealed in the mean profiles, the daily mean velocity and temperature profiles exhibited a considerable degree of uniformity throughout the observation periods.

The mean temperature and N^2 profiles obtained for the October observation exhibit several significant features. The main tropopause is seen to occur at $\sim$17 km, coincident with a large increase in stability. However, there is also a zone of high stability (a secondary tropopause) located at $\sim$10.5 km and which has a corresponding maximum in N^2 equaling stratospheric values above. The stability decreases approximately linearly above $\sim$3 km, becoming nearly adiabatic near 9 km. Above the N^2 maximum at 10.5 km there is a zone of several km depth in which the stability is approximately midway between the tropospheric and stratospheric values.

The November mean temperature and N^2 profiles differ from those for the early October observation in several respects. Perhaps the most significant difference is that the November profiles do not exhibit a secondary tropopause. Instead, these profiles show a gradual increase in stability between $\sim$12 and 18 km from a larger and more uniform tropospheric value to a comparable stratospheric value. These profiles are typical for Japan at this time of the year.

3. Fluctuations of velocity and temperature

We present in this section a discussion of the fluctuating components of the velocity and temperature fields occurring during the October and November observations. Our purpose here is to exhibit some of the variability of the motion spectrum, to identify the dominant contributions to the wave spectrum in frequency and wavenumber, and to estimate the amplitudes of individual wave motions relative to those required for linear instability of the wave field.

a. October data

To illustrate the fluctuating components of the velocity field, we present in Figs. 3 and 4 the daily means and the hourly averaged radial velocity fluctuations in the zonal and meridional directions for 17/18 and 24/25 October. Both figures exhibit a clear dominance of the wave spectrum by motions with vertical wavelengths of 2–3 km, primarily above the jet maximum. The similar amplitudes and the apparent phase quadrature of the zonal and meridional components provide clear indications that these motions are upward propagating gravity waves (a velocity vector rotating clockwise with height) occurring near the inertial frequency. Also seen clearly in Fig. 3 is a distinct downward phase progression of the low-frequency motion above the jet.

Below the jet maximum, there is evidence of wave motions as well, particularly in the meridional component. Here, however, the clear phase relationship evident above the jet is not as conspicuous. Wave amplitudes below the jet appear to be larger in the meridional component than in the zonal component of the motion field and appear to be especially large on 17/18 October near the level at which the early October temperature data exhibit a pronounced maximum in the mean stability due to a secondary tropopause. This

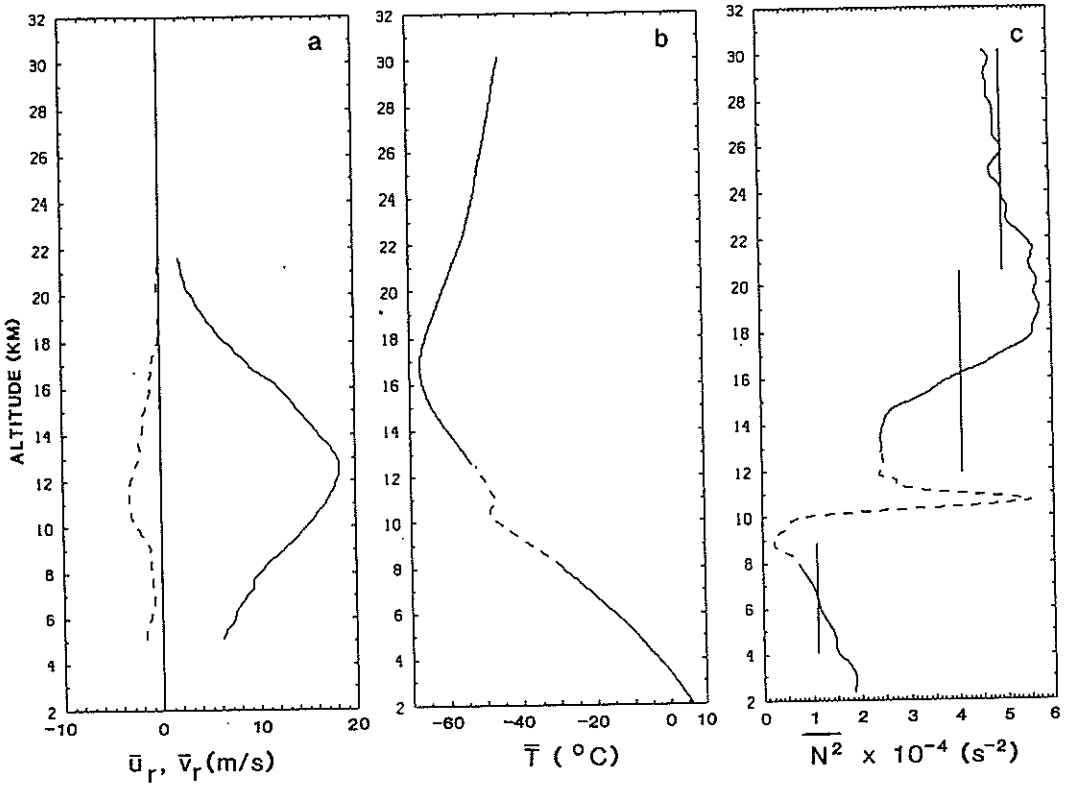

FIG. 1. Mean (a) eastward (solid) and northward (dashed) radial velocity, (b) temperature, and (c) N^2 profiles for the October observation. The velocity data cover the period 18–25 October. The temperature and stability data are for 20–22 October. Because of the limited number of profiles, a 3 km running mean was applied, except for the dashed portions of the temperature and N^2 profiles. Vertical bars on the N^2 profile show the mean values of N^2 and the height ranges used in spectral calculations. Note that mean radial velocities are smaller than inferred horizontal velocities by ~3. Units of N are rad s^{-1}.

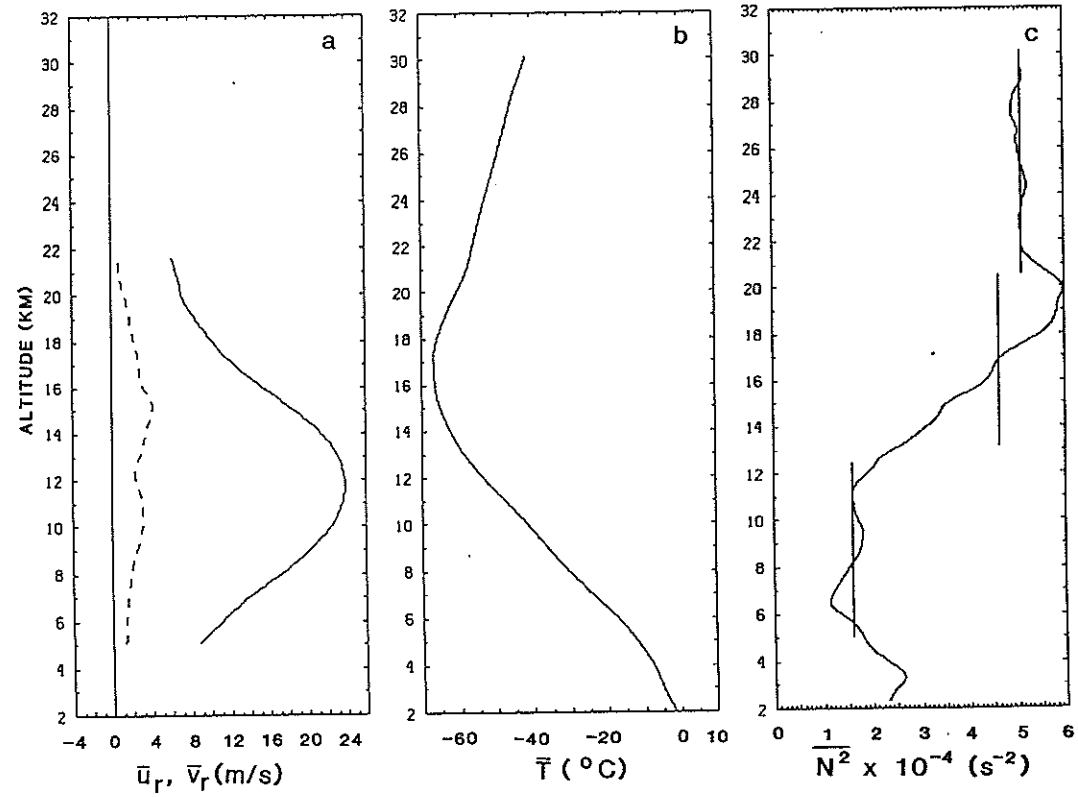

FIG. 2. As in Fig. 1, but for 26–29 November observation.

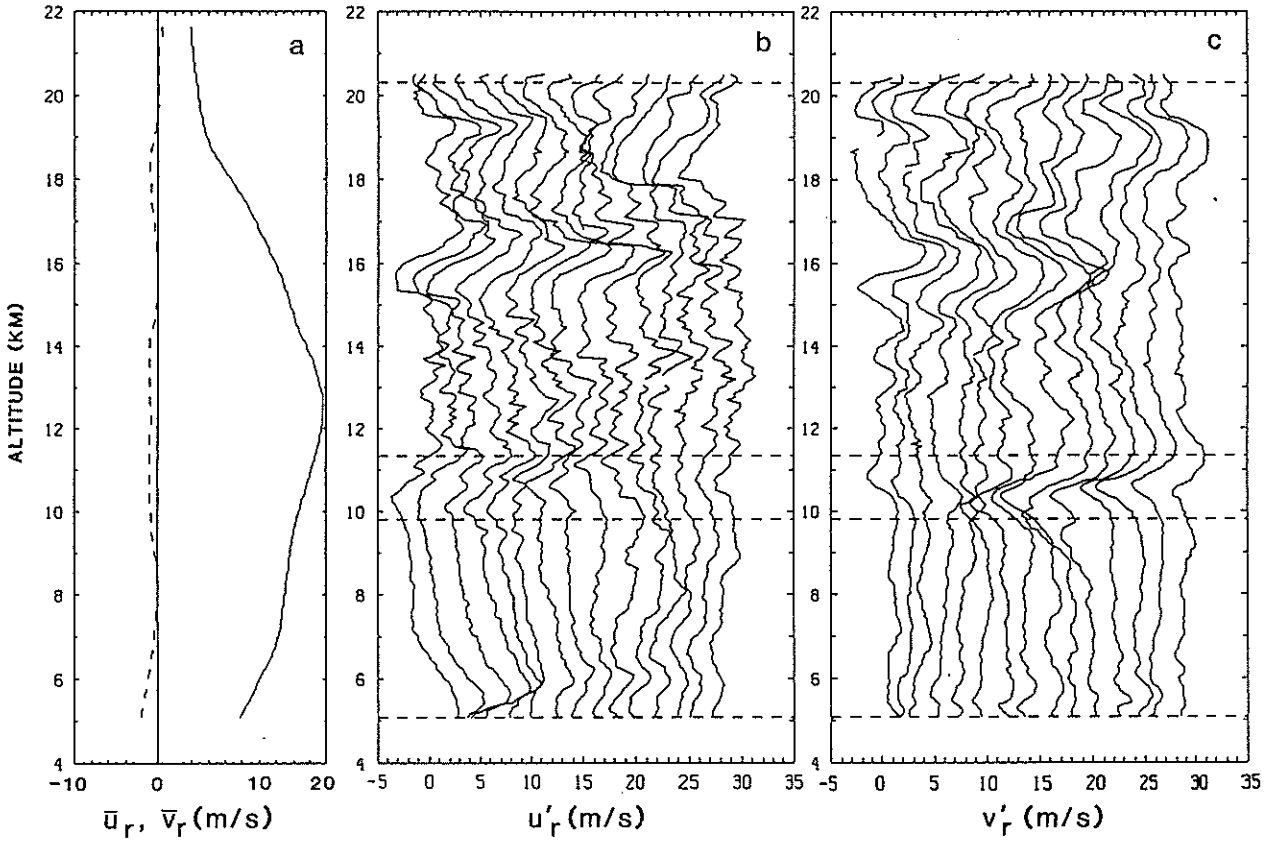

FIG. 3. Daily mean (a) eastward (solid) and northward (dashed) radial velocity profiles and hourly mean radial velocity fluctuations in the (b) east and (c) north directions for 17/18 October. Note the clear quadrature and downward phase progression of the eastward and northward velocities at larger vertical wavelengths above the jet. Dashed lines in (b) and (c) show the limits of the spectral calculations and successive profiles are displaced by 2 m s^{-1}.

is consistent with our expectation that the wave energy density will be larger in regions of enhanced stability due to the decrease in vertical wavelength (and vertical group velocity) and the requirement of a constant vertical energy flux for conservative motions with constant intrinsic frequency,

$$c_{gz}E = \text{const}, \tag{1}$$

where c_{gz} is the vertical group velocity and E the energy density. There is an apparent upward phase progression of the wave motion at this level, suggesting a downward propagation of this motion below the jet.

Also apparent in the zonal velocity profiles presented in Figs. 3 and 4 are small-scale structures with significant amplitudes near the core of the jet (~11–15 km). We believe, however, that this structure is an artifact of the broad beam width (~2.5° two-way), the 20° off-vertical angle, and the large zonal velocity at these heights. This "finite volume" effect causes an individual scattering layer to yield different radial velocity estimates in closely spaced range gates, contributing large vertical shears and inferred amplitudes (Fukao et al. 1987). Because of this contamination of the zonal velocities at high wavenumbers, we exclude the zonal velocity data from our spectral analyses in the following sections.

The temperature fluctuations and stability profiles inferred from the two balloon soundings during the night of 24/25 October are shown in Fig. 5. The temperature profiles reveal a clear ~2 km wave structure between ~15 and 19 km that appears to correlate well with the dominant motion seen in this height range in Fig. 4. This relation is explored further in Fig. 6, where the bandpassed velocity and temperature data for these soundings are presented together to permit a determination of the phase relationship. Illustrated here also are the wind hodographs (indicating a clockwise rotation of the velocity vector) and the cross-correlations of velocity and temperature. These results indicate that the most negative temperature gradients correlate best with wave velocities in a direction ~ 10° to 40° west of north, suggesting that the inertia–gravity wave had a nearly northward direction of propagation. The component of propagation against the flow is also consistent with the slow phase progression and the long inferred period of this motion.

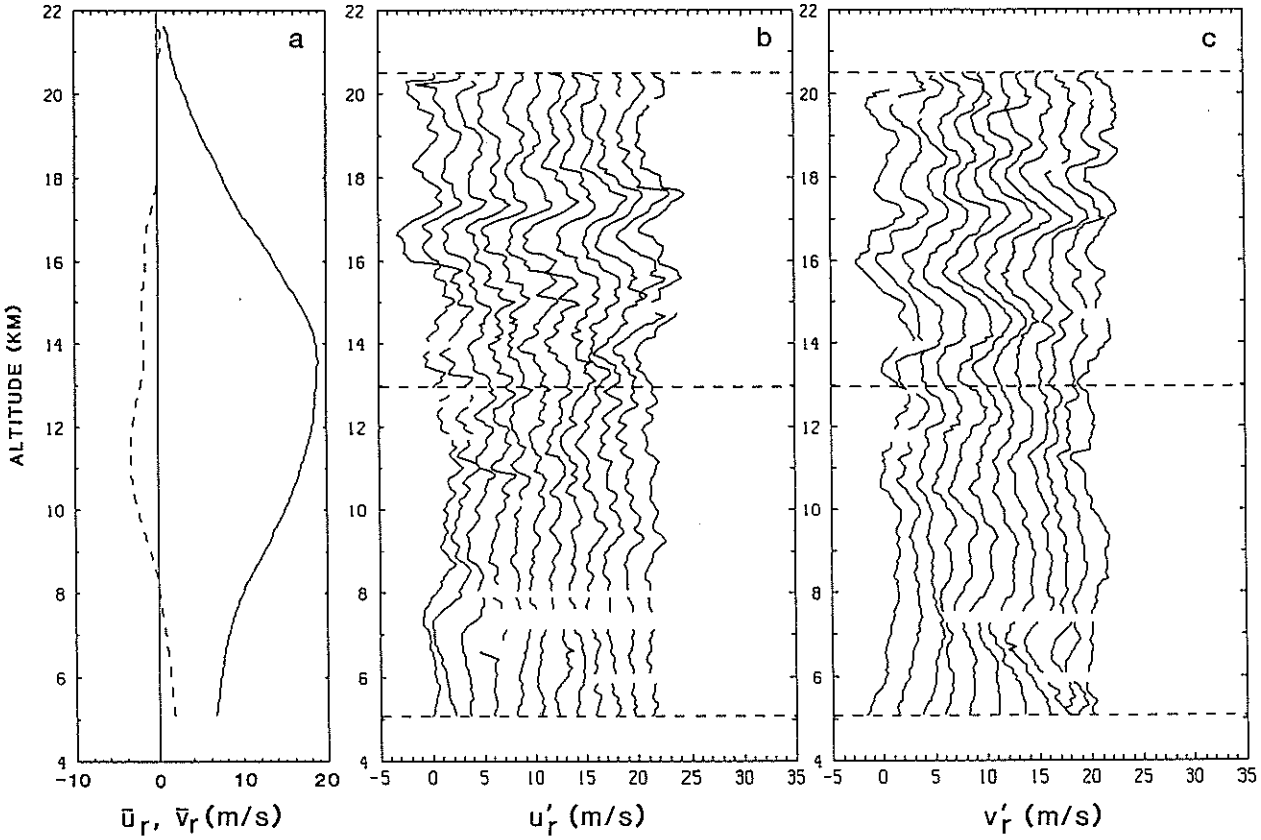

FIG. 4. As in Fig. 3, but for 24/25 October.

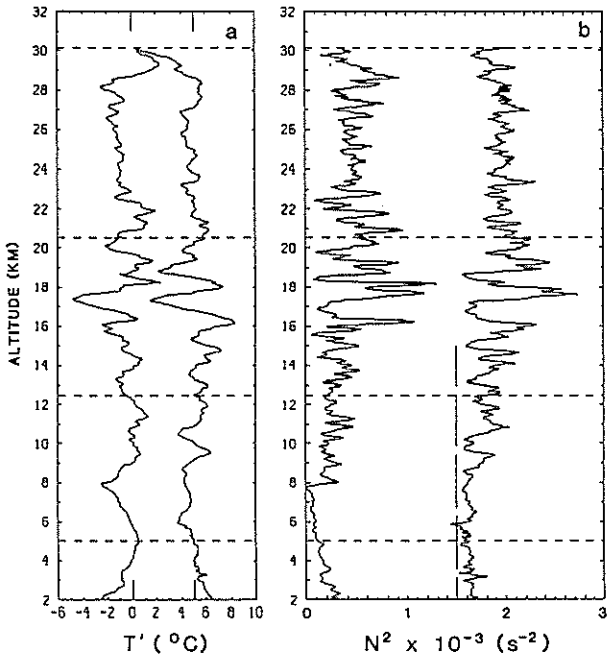

FIG. 5. Vertical profiles of (a) temperature fluctuations and (b) N^2 for the two balloon soundings on 24/25 October. Note the correspondence between the temperature and N^2 fluctuations between 15 and 19 km.

Wave amplitudes may be estimated from either the velocity or the temperature data. Because it is difficult to determine the intrinsic frequency accurately from the velocity data, however, the temperature data may provide the most reliable estimate for motions with intrinsic frequencies near f (the inertial frequency). From Fig. 5b we note that major fluctuations in N^2 are ~70% in the lower stratosphere, suggesting a wave amplitude of

$$\theta'_z/\bar{\theta}_z = u'/(c - \bar{u}) \sim 0.7, \qquad (2)$$

where θ is potential temperature, u' and $\bar{u}$ the horizontal wave perturbation and mean velocities in the direction of wave propagation, c the horizontal phase speed, primes and overbars denote perturbation and mean quantities, and subscripts denote differentiation. A value of 1.0 in Eq. (2) is required for a wave motion to be convectively unstable. However, low-frequency motions may also be unstable to dynamical instabilities at smaller amplitudes.

If we assume, due to the small vertical group velocities of such motions, that the observed amplitude of the wave in the temperature field is just that required for dynamical instability, we can infer the intrinsic frequency of the motion. An amplitude of 0.7 in Eq. (2) corresponds to the marginal amplitude for dynamical

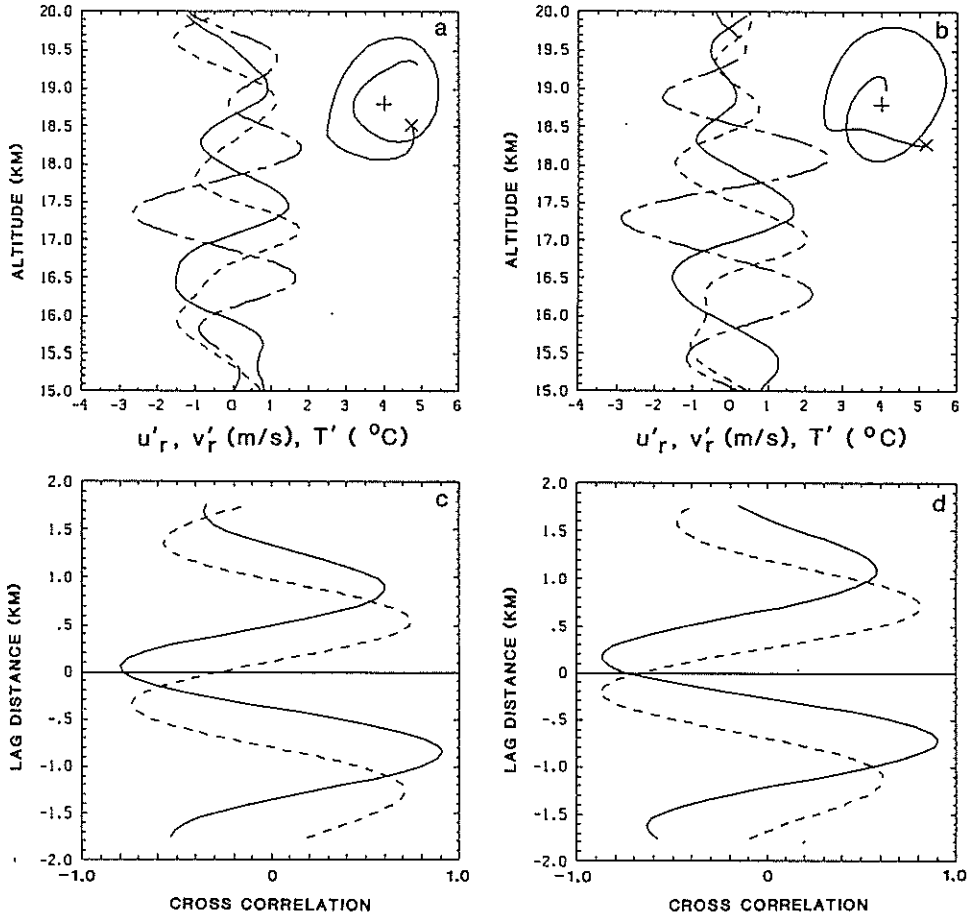

FIG. 6. Band-passed (0.9–3.6 km) fluctuations of temperature (short-long dashed) and of the corresponding eastward (solid) and northward (dashed) radial velocities for the balloon soundings of (a) 2100 and (b) 0200 LT on 24/25 October. Wind hodographs illustrate the clockwise rotation of the wind vector with height. Also shown are the cross-correlations of temperature with (c) eastward (solid) and (d) northward (dashed) velocity, indicating a vertical wavelength of ~1.8 km and a direction of propogation ~ 10°–40° west of north.

instability (Ri < ¼) for a motion with $f/\omega \sim 0.84$ (see Fritts and Rastogi 1985). This estimate is consistent with our observations of comparable zonal and meridional wave amplitudes and of quadrature between the two components. Even if our assumption of a marginal saturation amplitude is incorrect and the wave amplitude exceeds that required for dynamical instability, this only pushes our estimate of the intrinsic frequency of the motion closer to f. Thus, near the inertial frequency, our estimate of ω is insensitive to uncertainties in wave amplitude.

The intrinsic phase speed can likewise be inferred either from Eq. (2) with a knowledge of u' or from the dispersion relation for low-frequency motions,

$$m^2 = \frac{k^2 N^2}{(\omega^2 - f^2)} \tag{3}$$

or

$$(c - \bar{u})^2 = \frac{N^2}{m^2} \frac{1}{(1 - f^2/\omega^2)}, \tag{4}$$

where k and m are the horizontal and vertical wavenumbers of the wave motion. From Eq. (2), with $u' \sim 7$ m s^{-1}, we estimate the intrinsic phase speed to be ~10 m s^{-1}. Alternatively, Eqs. (3) and (4) allow us to estimate k and $(c - \bar{u})$ given N^2, ω, and $m = 2\pi/\lambda_z$. With the values cited above, this yields a horizontal wavelength $\lambda_x = 2\pi/k \sim 735$ km and an intrinsic phase speed of ~12 m s^{-1}, in reasonable agreement with the estimate obtained from Eq. (2). This procedure is simpler at higher intrinsic frequencies, where $k^2/m^2 = f^2/\omega^2 \ll 1$ and the intrinsic phase speed is then inversely proportional to the vertical wavenumber.

b. November data

Wind and temperature fluctuations, and several of the corresponding N^2 profiles, encountered during the 60-h November observation are illustrated in Figs. 7 and 8. The zonal and meridional radial velocity profiles were computed in ~1-h intervals. Temperature fluc-

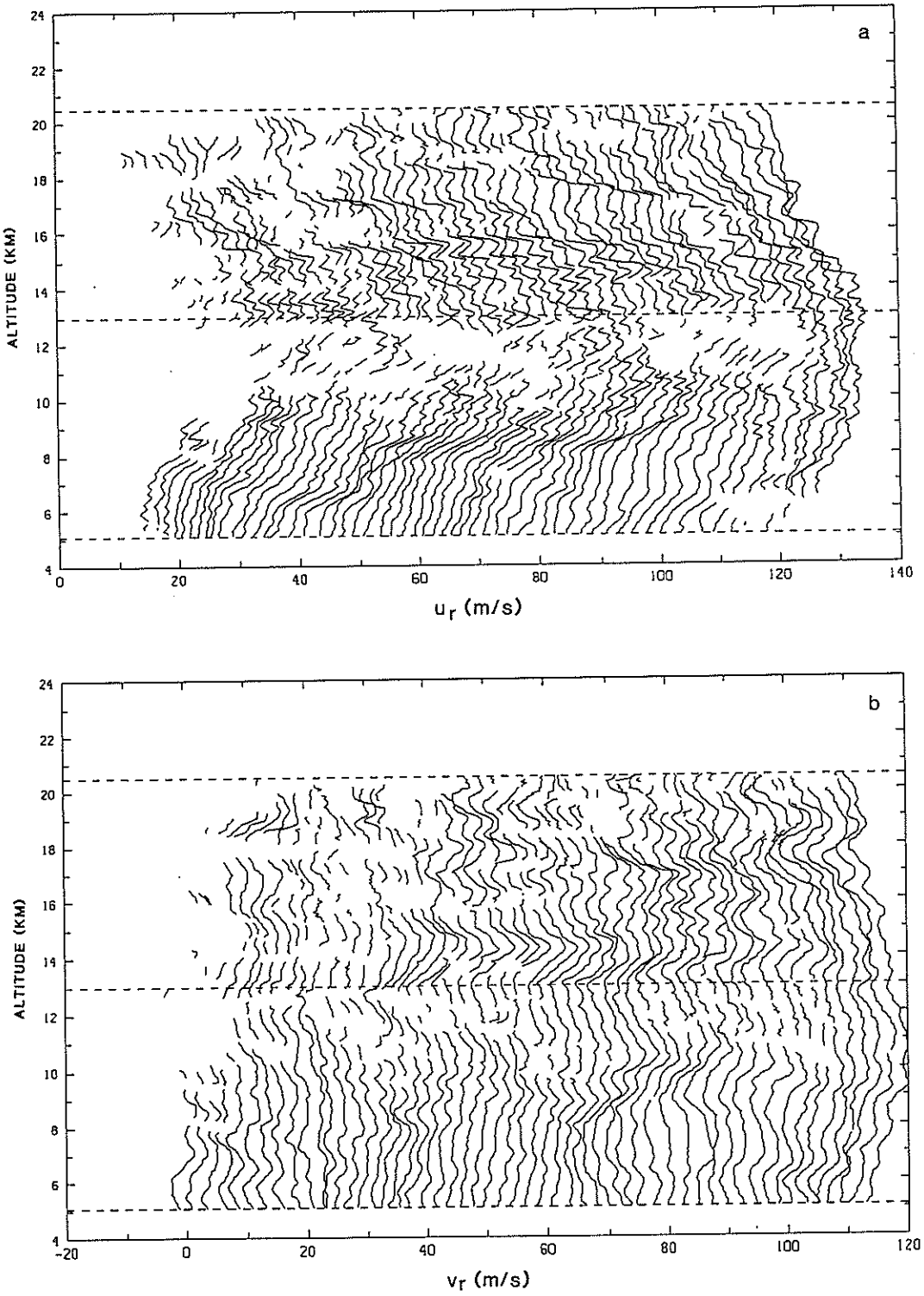

FIG. 7. Hourly mean profiles of (a) eastward and (b) northward radial velocity for the 26–29 November observation. Note the phase quadrature and downward phase progression of the dominant vertical scales above the jet and the upward and downward phase progressions below the jet. Successive profiles are displaced by 2 m s^{-1}.

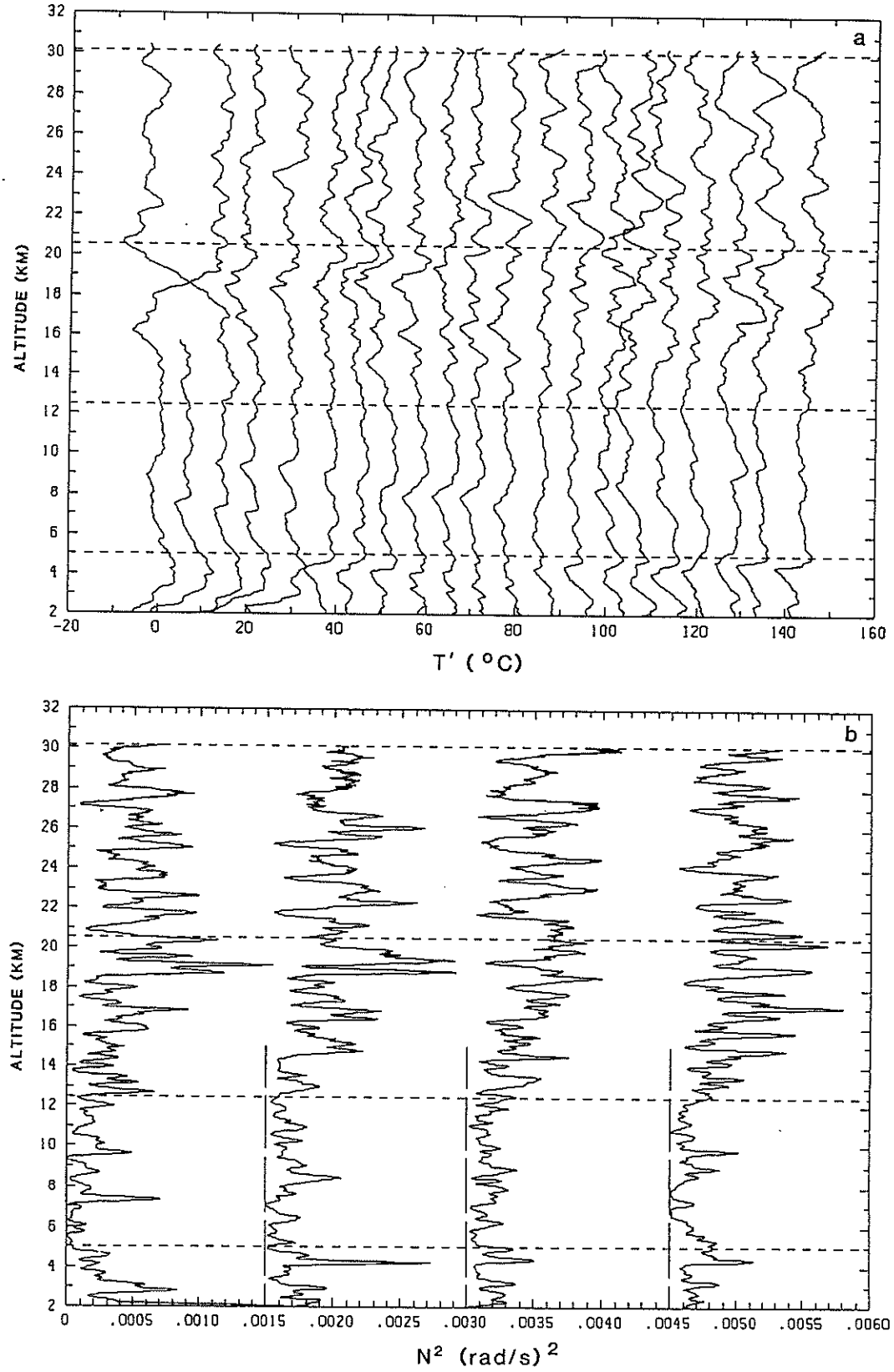

FIG. 8. Fluctuations (a) of temperature for the 21 soundings at ~3-h intervals during the November observation and (b) of N^2 for soundings 3, 8, 13 and 18. Note the phase progressions in the temperature data and the variations of vertical scale and amplitude with height and time in the N^2 profiles. Successive profiles are displaced by 7 K and 0.0015 (rad s^{-1})^2, respectively

tuations about the mean were computed for soundings performed every 3 hours. The resulting dataset reveals a rich array of wave motions. As seen in the October dataset, both velocity and temperature fluctuations are dominated by ~1–3 km vertical wavelengths, with considerable variability across the jet structure and between the troposphere and stratosphere. Because of their dependence on vertical gradients, the N^2 profiles tend to emphasize the structures at smaller vertical scales.

Perhaps because of the more continuous data base, phase progressions appear to be more clearly defined during the November observation. This is particularly true in the hourly velocity data, where wave motions with vertical wavelengths of ~1–3 km are prevalent. As noted in the October data, the larger vertical scales exhibit quadrature between the zonal and meridional components and there is a clear tendency for downward phase progression above the jet. There is evidence of both upward and downward phase progression below the jet. As seen in the October data, there are also small-scale features in the zonal velocity component within the jet due presumably to the finite volume effect which we believe are not representative of the true velocity field. As confirmation of this, we note that vertical scales of temperature fluctuations correlate well with those of velocity fluctuations only in the meridional direction. Also noted is a tendency for zonal velocity data to be missing near the core of the jet. This is a result, not of low S/N, but of an aliasing of the zonal velocity estimates because of a narrow spectral window. Finally, there is a tendency for wave amplitudes to achieve larger values in the stratosphere than in the troposphere. It will be shown in the following section that this is a result of the increased stability and thus of the larger saturated amplitudes in the stratosphere.

The temperature and N^2 profiles shown in Fig. 8 likewise exhibit a number of interesting features of the wave spectrum during November. As noted in the velocity data, the spectrum is dominated by vertical wavelengths of ~1–3 km, with the larger-scale structures having larger temperature fluctuations. Large fluctuations occur primarily below 5 km and above ~15 km, corresponding to those regions with large stability. In contrast, temperature fluctuations between 5 and 15 km are much less significant. Variations in N^2, on the other hand, appear to scale with N^2 and are contributed by a broader range of vertical wavelengths. The scaling of wave amplitudes with stability presented in the next section will be shown to account for many of these features. Also seen in the temperature data are phase progressions consistent with those noted in the velocity data. These are generally downward above the jet and both upward and downward below.

4. Vertical wavenumber spectra of velocity and temperature

We examine in this section the dominant vertical scales implied by the observed vertical wavenumber spectra, the variability of these spectra in time, the consistency between the temperature and velocity data, and the extent to which the data support the saturation theory of Dewan and Good (1986) and Smith et al. (1987). To motivate this discussion, we briefly review the saturation theory and its implications for our velocity and temperature data.

a. Linear saturation theory

Both Dewan and Good (1986) and Smith et al. (1987) argued that the saturation of individual wave motions by convective or dynamical instabilities would lead to a saturated power spectral density (PSD) of the form

$$F_u^s(m) \approx b\frac{N^2}{m^3}, \tag{5}$$

where u denotes a velocity spectrum, s denotes saturation, and b is a coefficient that depends on the shapes of the vertical wavenumber and frequency spectra of gravity wave motions. Using the relation

$$\left|\frac{T'}{\bar{T}}\right| = \left|\frac{\theta'}{\bar{\theta}}\right| = \frac{u'}{(c-\bar{u})}\frac{N^2}{mg}, \tag{6}$$

where g is the acceleration due to gravity, together with the dispersion relation given by Eq. (2), the corresponding saturated PSD for normalized temperature $(T'/\bar{T})$ may be written

$$F_T^s(m) = d\frac{N^4}{g^2m^3}, \tag{7}$$

where d will differ from b, in general, due to the reduction of potential energy relative to kinetic energy for wave motions with intrinsic frequencies near f.

The most direct means of obtaining the saturated PSDs of velocity and normalized temperature is by assuming

$$\overline{\theta_z'^2} = \bar{\theta}_z^2/2 \tag{8}$$

for marginal wave field instability and integrating the contributions to the variance of potential temperature gradient over all m. For a vertical wavenumber spectrum of the form seen to be appropriate in previous oceanic and atmospheric studies (Desaubies 1976; Fritts and Chou 1987),

$$F_{u,T}(m) \sim \frac{1}{(1+(m/m_*)^t)}, \tag{9}$$

with $t = 3$ and m_* a characteristic vertical wavenumber. With reasonable estimates of the characteristic and maximum vertical wavenumbers of the gravity wave spectrum, this yields $d \approx 0.1$. Also assuming that the total wave energy varies as ω^{-p} with $p \approx \frac{5}{3}$ (Balsley and Carter 1982), this yields a coefficient for the saturated PSD of horizontal velocity of $b \approx pd \approx \frac{1}{6}$ (Smith et al. 1987).

Both saturated PSDs have amplitudes that vary as m^{-3}, but the amplitude of the normalized temperature spectrum is much more sensitive to changes of N^2 with height. These spectra provide not only a means of testing the validity of the linear saturation theory, but also permit us to examine the degree to which the temperature and velocity data are consistent with the gravity wave interpretation of atmospheric motions. Such consistency may not preclude other possible explanations of the motion field, however.

We have elected to present normalized temperature spectra to remove the influence on the spectral power of a mean temperature varying with height. In Eqs. (5) and (7), N and m have units of rad s^{-1} and rad m^{-1}, respectively. For convenience, however, power spectra of radial velocity and normalized temperature will be presented versus inverse wavelength in units of cycles per meter (cpm).

As noted above, the coefficients in Eqs. (5) and (7) will differ, in general, depending upon the intrinsic frequency composition of the wave spectrum. Yet our knowledge of the distribution of gravity wave energy at intrinsic frequencies near f is poor at present. We do know from the observed wave structure seen in the previous section and in other studies, however, that the spectrum includes significant power near inertial frequencies. Thus, it is important to comment on the possible influence of these effects.

The relative magnitudes of the kinetic and potential energies of the gravity wave spectrum depend on the wave amplitudes, and thus on those processes acting to limit wave amplitudes, at low intrinsic frequencies. It can be shown that the amplitude required for dynamical instability of the wave field (assuming Ri = ¼) varies with intrinsic frequency as (Fritts and Rastogi 1985)

$$\frac{u'}{(c-\bar{u})} = \frac{\theta_z'}{\bar{\theta}_z} = \frac{2(1-f^2/\omega^2)^{1/2}}{1+(1-f^2/\omega^2)^{1/2}}, \qquad (10)$$

which falls to zero at the inertial frequency. The corresponding amplitude required for convective instability in Eq. (10) is 1.0 for all ω. Because we are interested in vertical wavenumber spectra, however, and the vertical wavenumber increases for constant $(c-\bar{u})$ as $f/\omega \rightarrow 1$, the saturated wave amplitude of the horizontal velocity spectrum at a fixed vertical wavenumber (assuming a dynamical instability) varies as

$$F_u^s(m) \sim \frac{u'^2}{m} = \frac{N^2}{m^3}\left[\frac{2}{1+(1-f^2/\omega^2)^{1/2}}\right]^2. \qquad (11)$$

A significant low-frequency component of the gravity wave spectrum would thus increase the saturated spectral amplitude of horizontal velocity given by Eq. (5), depending on the integrated contributions of low- and high-frequency motions. Another factor that contributes to the increase in this spectral amplitude at low frequencies is the transverse velocity of wave motions propagating in a perpendicular direction. In contrast, the contribution to the normalized temperature variance due to motions limited by dynamical instabilities at low frequencies is reduced below that value given by Eq. (7) with $d \approx 0.1$ by the square of the factor given by Eq. (10). Thus, while the structure of low-frequency wave motions tends to increase the ratio of kinetic to potential energy in the wave field, the apparent importance of the dynamical instability at low intrinsic frequencies may act to reduce these wave amplitudes and their contributions to a departure from equipartition of energy within the wave spectrum. Consequently, the ratio of coefficients in Eqs. (5) and (7) may differ from p and will, in any event, depend on the distribution of wave energy with intrinsic frequency.

While power spectra in the form of Eq. (9) permit us to compare asymptotic spectral slopes and amplitudes with the predictions of saturation theory, in order to infer the relative contributions to the variance of the spectra or the dominant vertical scales, it is more convenient to present the spectra in an area-preserving form. If the quantity $mF(m)$ is plotted on a linear scale versus $\log m$, the relative contributions to the variance are proportional to the area under the curve. With $F_u(m)$ given by Eq. (9), the mode of $mF(m)$ lies at $\lambda_b = m_*/2^{1/3}$. Since most of the energy lies within a factor of 3 of the mode, the observed dominant vertical scale will correspond closely to λ_b.

b. *October spectra*

The October data provide a convenient way to examine the consistency, dominant scales, and daily variability of the wave spectrum observed in the velocity and temperature fields. To illustrate this, we first present the power spectra of zonal and meridional radial velocity and normalized temperature for 24/25 October between 13 and 20.5 km in Fig. 9. This is the period and the height range in which a well-defined, coherent wave structure was identified in these data (see Fig. 6).

Let us first consider the usual log–log plots of the power spectra shown in the top panels. The saturated spectra predicted by the linear saturation theory are shown as dashed straight lines with a slope of −3. Note that the predicted saturated amplitude of the velocity spectrum has been reduced by $\sin^2(20°)$ to allow for comparison with the radial velocity spectra. Clearly, there is excellent correspondence between the predicted saturated spectra and the observed spectra, in both shape and amplitude. Both the velocity and normalized temperature spectra exhibit clear breaks in the slopes to less negative or even positive values at small wavenumbers, as noted in the stratospheric data of Fritts and Chou (1987). They also both have a spectral gap at ~1 km ($m \sim 10^{-3}$ cpm) providing further evidence that the two fields are dynamically related. These spectra do exhibit considerable variability, however, and should not be viewed as representative of average

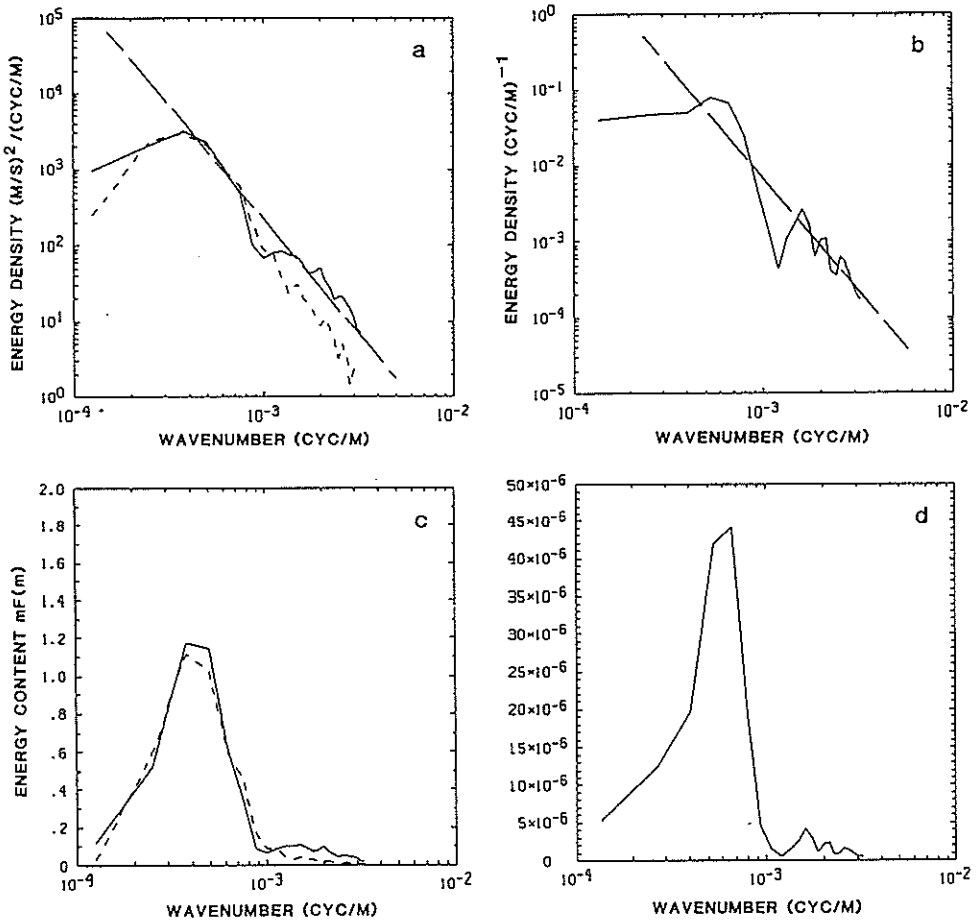

FIG. 9. Power spectral densities (PSD) (a) of eastward (solid) and northward (dashed) radial velocity and (b) of normalized temperature between 13 and 20.5 km for 24/25 October and the corresponding area-preserving spectra (c) of radial velocity and (d) normalized temperature. Long dashed lines show the saturated PSDs predicted by Eqs. (9) and (10). Note the similarities in spectral shape, with a spectral gap near 1 km ($m \sim 10^{-3}$ m^{-1}), and in the dominant vertical wavenumber in the area-preserving spectra.

conditions. The average spectra and their scaling with N^2 will be addressed in the next section.

Now let us consider the area-preserving plots in the lower panels of Fig. 9. The dominant vertical scale in the velocity field is seen to be ~2.5 km and that in the temperature field ~ 2 km, which is very good agreement considering that the velocity data represent a 16 h average whereas the temperature data were obtained from only two soundings. They also agree very well with the value of ~2.3 km reported by Fritts and Chou (1987), and they confirm the relatively small characteristic vertical scales of the wave spectrum in the lower stratosphere inferred by Smith et al. (1987). Finally, the consistency of the observed spectra with the saturated spectra and the agreement of the dominant scales and shapes of the velocity and temperature spectra provide further support for the view that fluctuations at these heights are due to atmospheric gravity waves.

We now use the area-preserving spectra of zonal and meridional radial velocities to examine the daily variability of the motion spectrum during the October observation. These spectra are shown for the height range from 13–20.5 km in Fig. 10. The results indicate that there were daily variations in the dominant vertical scale of the wave spectrum, the total wave energy, and the relative energy of the zonal and meridional components. The dominant vertical scale, λ_b, remained near ~2.5 km throughout the period, with smaller values occurring during the nights of 20/21, 21/22, and 24/25 October. With the exception of 23/24 October, there was also agreement of the dominant vertical scale inferred in the zonal and meridional component on each night. The total (radial) wave energy (proportional to the area under the area-preserving spectrum) decreased by ~3 between 17/18 and 21/22 October and increased by the same factor thereafter. Finally, the relative magnitudes of the zonal and meridional (radial) energies suggest that there was some variability

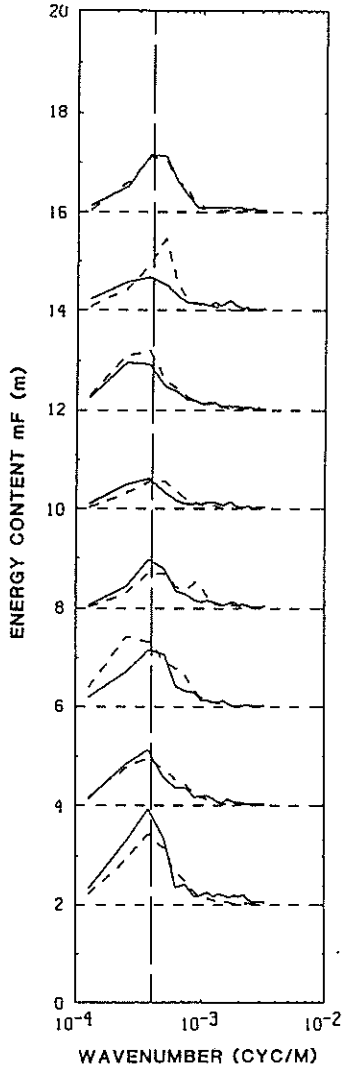

FIG. 10. Daily averaged area-preserving spectra of eastward (solid) and northward (dashed) radial velocity between 13 and 20.5 km for the October observation. Note the variations in variance and dominant vertical wavenumber. The dashed vertical line indicates a wavenumber of 4×10^{-4} m^{-1} ($\lambda_z = 2.5$ km) for reference.

in the dominant direction of wave propagation during this period, with propagation more nearly aligned with the zonal flow at early times and in the meridional direction during the latter part of the observation period.

c. *November data*

To examine the variability of the motion spectrum on time scales less than a day, we present in Figs. 11 and 12 the area-preserving spectra of meridional radial velocity and normalized temperature at ~1-h and 3-h intervals, respectively, throughout the November observation. The radial velocity spectra were computed for height ranges of 5–13 and 13–20.5 km. Normalized temperature spectra were computed for height ranges of 5–12.5, 12.5–20.5, and 20.5–30 km for the 20 soundings that achieved heights $\geq$ 20 km. To insure that the velocity spectra were not biased by variations of the mean wind, a 21-h running mean of the velocity data was removed from each profile. We also considered only the meridional component of velocity to avoid contamination of the results by the high-wavenumber structure near the jet core due to the broad radar beam width. This yielded 37 1-h velocity profiles from which area-preserving spectra were computed.

The area-preserving spectra of meridional radial velocity shown in Fig. 11 display a remarkable consistency from one sounding to another and clearly show the variations of wave energy and of the dominant vertical scale with time. Because of the smaller energy densities [due to a smaller N^2, see Eq. (5)], the tro-

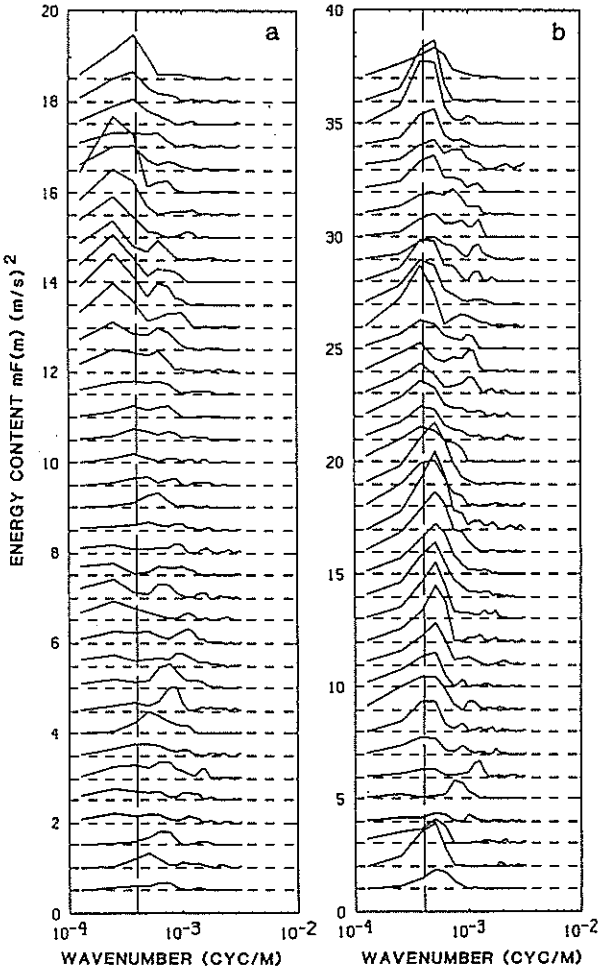

FIG. 11. Hourly area-preserving spectra of northward radial velocity for (a) 5–13 and (b) 13–20.5 km during the November observation. Only 37 profiles were computed in order to remove a 21-h running mean from each profile. Note the consistency in time and the variations in energy and dominant vertical wavenumber. The dashed vertical line indicates a wavelength of 2.5 km for reference.

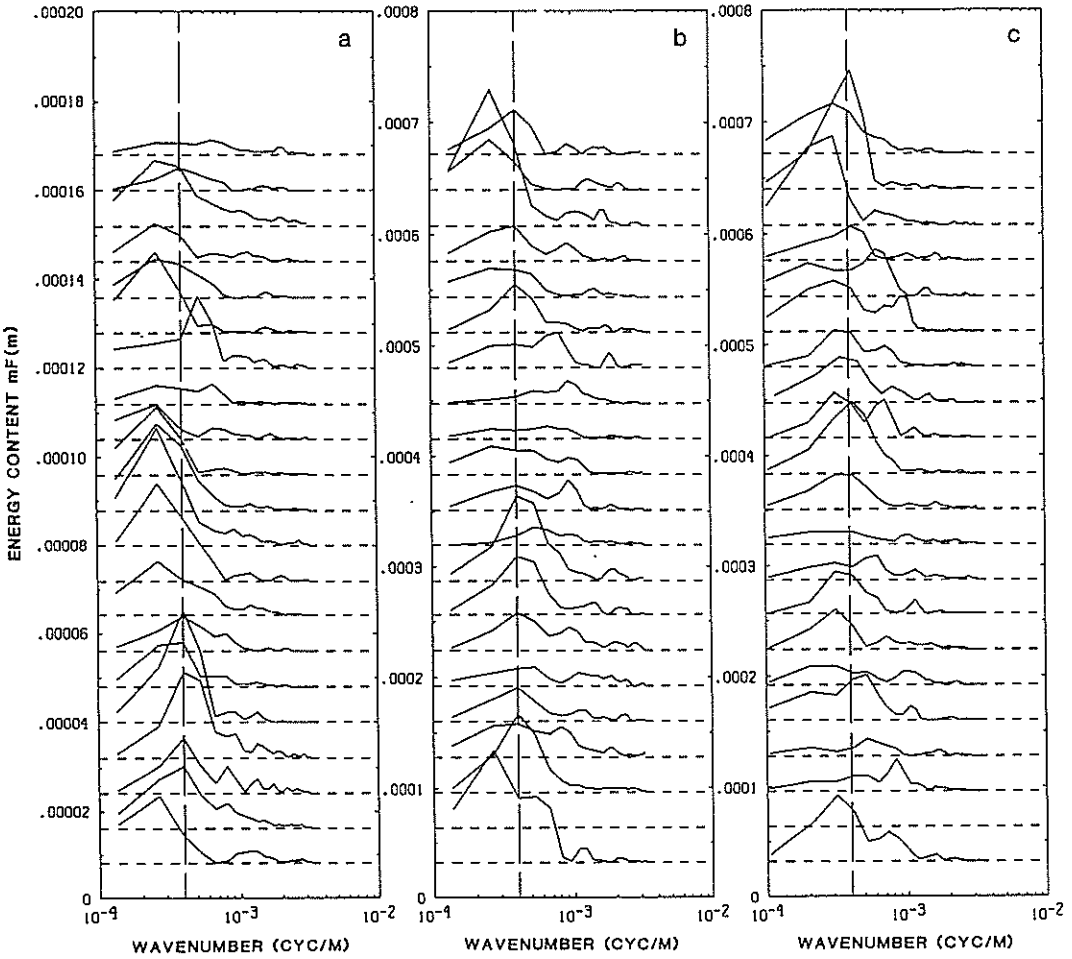

FIG. 12. Area-preserving spectra of normalized temperature for (a) 5–12.5, (b) 12.5–20.5, and (c) 20.5–30 km during the November observation. Note the correspondence with the area-preserving spectra of radial velocity in the stratosphere between soundings 5 and 17.

pospheric values have been enhanced by a nominal factor of 2 relative to the stratospheric values for ease of comparison. There is considerable variability of the energy and the dominant scale in both the troposphere and lower stratosphere on time scales of a few hours, suggesting that there is a significant high-frequency component of the motion field in addition to the inertia–gravity wave motions noted earlier. There is also remarkably little correlation between the energies and the dominant vertical scales from the troposphere to the stratosphere. This suggests that the jet itself, rather than the troposphere below, may be a significant source of wave motions in the lower stratosphere.

Tropospheric energy in the meridional radial velocity was small and distributed over a broad range of wavenumbers during the early and middle portion of the November observation, with a significant increase in both energy and scale occurring near the end. In contrast, the stratospheric area-preserving spectra exhibit several distinct maxima of ~2–15 h duration, more narrowly confined energies in vertical wavenumber, and secondary maxima that display some temporal consistency. Like the October results discussed previously, the dominant vertical scale varies between ~2 and 3 km. Secondary maxima, on the other hand, occur at vertical scales of ~1 km or less. In the lower stratosphere, these secondary maxima also tend to follow more energetic periods characterized by larger dominant vertical wavelengths.

The area-preserving spectra of normalized temperature shown in Fig. 12 exhibit similar variability to the velocity spectra. It must be noted, however, that the temperature data cover an interval of ~60 h while the velocity data presented in Fig. 11 cover only ~40 h, corresponding to the temperature spectra for soundings ~ 5–17. Given this, there is reasonable agreement between the gross features of the temperature and velocity spectra in the lower stratosphere, with the four temperature maxima in profiles 5, 7–9, 11–12, and 16–17 corresponding to the four maxima seen in the strato-

spheric velocity data. This suggests sufficient low-frequency wave energy to insure that the radar and the balloons, despite their downstream advection, respond to essentially the same wave field.

The tropospheric area-preserving spectra of normalized temperature (enhanced by a factor of 4 to permit a comparison with the stratospheric spectra) exhibit significant variability and appear to be weakly correlated with those fluctuations in the lower stratosphere. There is, in addition, very little correlation of these spectra with the tropospheric wind spectra, suggesting that they are more representative, perhaps, of processes or structures other than wave motions in this region. There is a correlation, however, between those times at which large values of the normalized temperature variance were observed in the troposphere and periods during which the large-scale temperature gradients were most negative. Thus it is possible that convection, rather than wave motions, contributed significantly to the spectral energy in the troposphere, and to the enhancement of the spectral energy in the stratosphere due to convective excitation of gravity waves, at these times.

The area-preserving spectra of normalized temperature exhibit a similar lack of correlation between the lower and middle stratosphere, except that the dominant scales and energies in these regions are comparable. This lack of a correlation is not unexpected, but may result from the dominance of the energy spectrum by low-frequency motions, their associated slow vertical propagation, and the likelihood that the jet is a source of this variable, low-frequency wave activity.

The temporal variability of the normalized temperature and radial velocity spectra described here reveal significant departures from the predicted mean saturated spectra. Variations that are consistent with predicted saturated amplitudes can occur if wave energies increase (decrease) in response to a decrease (increase) of m_* (Smith et al. 1987). Variability can also occur, however, as noted in the discussion of Fig. 9, when certain wavenumbers or frequencies contribute preferentially to the motion field. As proposed by Dewan and Good (1986) and Smith et al. (1987), the saturated spectral amplitudes are determined by the integrated variance of all wavenumbers and frequencies. Thus, if certain components of the spectrum are weak or absent, others must contribute to a greater degree. Finally, the predicted saturated spectrum represents an idealized, equilibrium spectrum, yet the atmospheric wave spectrum is dynamically active and temporally variable. As such, we should expect departures from the mean spectrum due to wave transience and random and variable occurrences of wave field instability.

5. Mean velocity and temperature spectra and N^2 scaling

We present in this section the mean spectral results of the November observation and the variance of meridional radial velocity and normalized temperature as functions of height. The mean spectra of radial velocity and normalized temperature are compared with the spectral slopes and amplitudes predicted by linear saturation theory and with the scaling of these amplitudes with N^2. Mean vertical wavelengths of the motion spectra are inferred from the area-preserving spectra. Finally, vertical profiles of the variances of radial velocity and normalized temperature are used to provide greater sensitivity to the varitions of N^2 with height.

Shown in Fig. 13 are the mean spectra and area-preserving spectra of the meridional radial velocity and normalized temperature for the November observation. Also shown for reference with the energy spectra are the predicted saturated amplitudes for the lower stratosphere given by Eqs. (5) and (7) with $N^2 = 0.00046\ s^{-2}$ inferred from Fig. 2. As in Fig. 9, the saturated amplitude given by Eq. (5) has been reduced by $\sin^2(20°)$ for comparison with radial velocity spectra. The small fluctuations in spectral amplitude at large wavenumbers are a result of the large number of individual spectra contributing to the mean spectra.

Several features of the mean spectra are significant. First, we note that both the spectral amplitudes and slopes at high wavenumbers in the stratosphere are in excellent agreement with those values predicted by linear theory, suggesting consistency between the two fields and providing strong support for the view that such motions are due to internal gravity waves. It should be mentioned here that our sensitivity only to motions with observed periods longer than ~2 h reduces spectral amplitudes by ~20%, assuming the frequency spectrum of horizontal motions had a $-5/3$ slope between f and N (Balsley and Carter 1982; Vincent 1984). Also seen in the energy spectra are clear differences in the spectral amplitudes between the troposphere and stratosphere, with the lower stratosphere having values for $m > 10^{-3}\ m^{-1}$ ($\lambda_z < 1$ km) that are larger by ~2.5 and 6.3 for the velocity and normalized temperature, respectively. These should be compared with predicted values, based on the ratio of N^2 in the two regions, of 2.88 and 8.27 if tropospheric motions were due entirely to gravity waves. We saw evidence in Figs. 10–12, however, that all tropospheric fluctuations may not be due to the gravity wave spectrum. Thus we should expect, because of the possibility of convective activity in the troposphere, somewhat smaller ratios of spectral amplitudes than predicted for a gravity wave spectrum alone.

The area-preserving spectra shown in Fig. 13 allow us to infer the mean vertical scales of the velocity and temperature fluctuations in the troposphere and stratosphere for the November observation. These values in the stratosphere are ~2.5 and 2.9 km, respectively, for the velocity and temperature data. Together with the consistency in spectral slope and amplitude and the scaling with N^2 noted above, this provides strong evidence that the two fields are dynamically re-

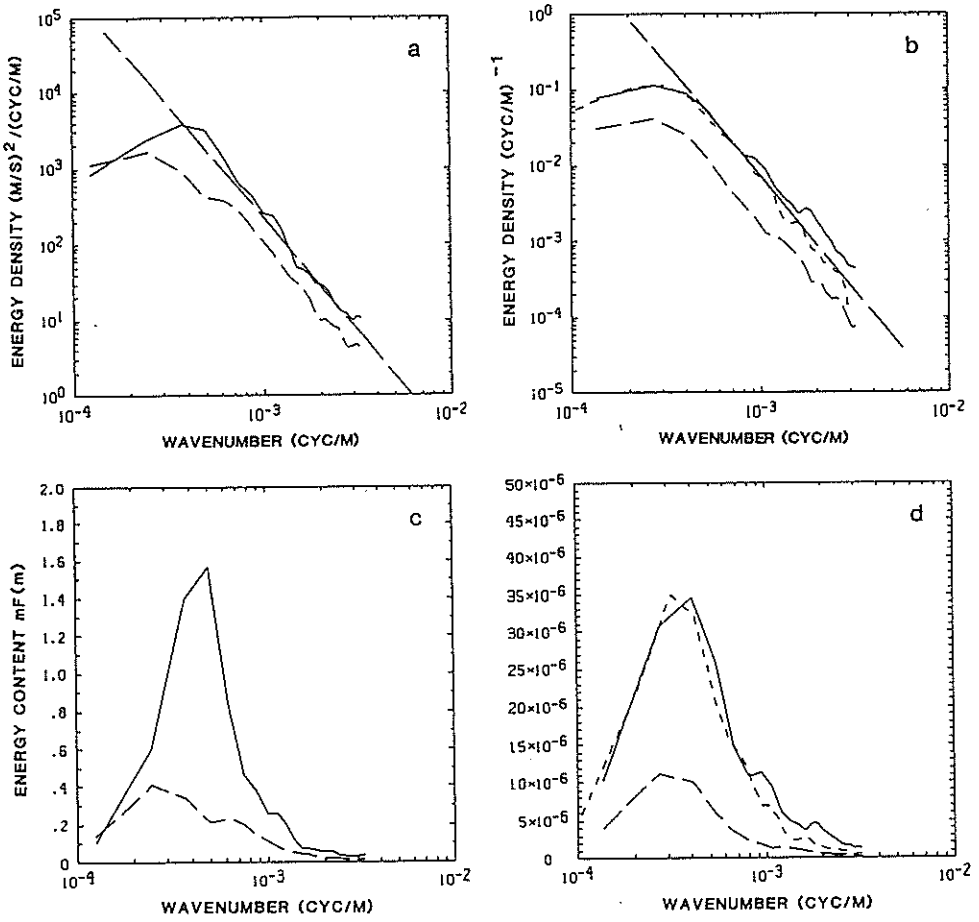

FIG. 13. Mean PSDs (a) of eastward plus northward radial velocity and (b) of normalized temperature at 5–12.5 (long-dashed), 12.5–20.5 (solid), and 20.5–30 (short-dashed) km heights. As in Fig. 9, the long dashed lines show the predicted saturated spectral amplitudes for the 12.5–20.5 km height range. Shown in (c) and (d) are the corresponding area-preserving spectra. Note the excellent agreement with the predicted amplitudes at high wavenumbers in the stratosphere and the similarity in the dominant vertical scale inferred from the velocity and temperature data.

lated via gravity wave motions. Also noted in the normalized temperature data is a tendency for slightly enhanced variance at the middle stratospheric heights, consistent with a further increase in N^2 above lower stratospheric values and a corresponding growth in wave amplitudes at the larger vertical scales. The tropospheric area-preserving spectra likewise yield estimates of the dominant vertical scales at these heights of ~2.5–3 km. But while consistent with those values noted in the stratosphere, we regard these estimates as less reliable because of the potential contamination due to convection in the troposphere. Finally, the mean area-preserving spectra provide clear evidence that virtually all of the velocity and temperature variance in the troposphere and lower stratosphere occurs at scales within a factor of ~3 of the dominant vertical scale.

The mean height profiles of radial velocity and normalized temperature variance, computed with a 3 km sliding window for the November observation are shown in Fig. 14. The velocity variance profile in Fig. 14a exhibits significant variations with height, with peaks occurring near 8 km and above ~13 km. In the troposphere that is seen to occur near and above the region of low mean stability and may be due in part to convection during periods when this region is unstable. The peak at greater heights coincides not with the N^2 maximum (see Fig. 2), but with the large N^2 gradient below 18 km, suggesting that there is an adjustment interval in which the wave spectrum achieves equilibrium with its new environment. Such an adjustment involving excess wave amplitudes and wave dissipation is expected on the basis of linear theory (VanZandt and Fritts 1988). A good correspondence is seen between the minima of mean velocity variance and N^2 near 11 km.

The mean vertical profile of normalized temperature variance shown in Fig. 14b is seen to be in qualitative agreement with the N^2 profile. Both exhibit a relative

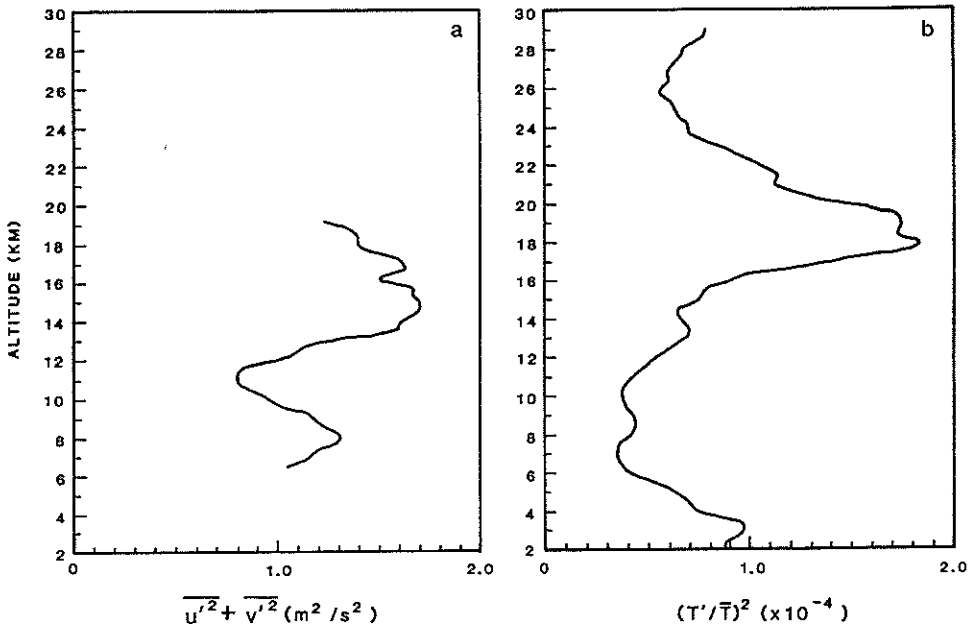

FIG. 14. Vertical profiles of (a) radial velocity and (b) normalized temperature variance. The variances were computed using a 3 km sliding window.

maximum at 3–4 km, a broad minimum between ~5 and 13 km, and a maximum near 18–20 km. Within the troposphere, even the small-scale variations are in approximate agreement. There is, nevertheless, greater variance than expected relative to peak values, perhaps as a result of convection and/or greater inherent variability of the mean structure in the troposphere. Greater variance fluctuations are anticipated if we assume conservative (nondissipative) wave propagation, in which case the velocity and normalized temperature variances would scale as N and N^3, respectively. But gravity wave saturation at high wavenumbers and enhanced saturation due to increases in N cause the measured variances to vary less rapidly in the atmosphere (VanZandt and Fritts 1988).

As noted in the mean velocity variance profile, the peak in the normalized temperature variance is displaced somewhat below the N^2 peak, perhaps in response to the same factors that led to the differences in Fig. 14a. Finally, we note a reduction in the variance above ~20 km relative to the peak value. However, this is seen to be an artifact of our 3-km window for variance computations as we see from Figs. 7a and 13d that there is significant variance at scales larger than 3 km and that the total variance in the 12.5–20.5 and 20.5–30 km heights ranges are virtually identical. The larger scales contributing variance at upper heights resulted from removal of the time-mean profile rather than from the 3-km smoothing of the mean temperature profile. Accounting for this variance at larger vertical scales brings the variance profile into close agreement with the N^2 profile above ~14 km.

6. Conclusions

We have presented an analysis of two datasets including vertical profiles of velocity and temperature collected with the MU radar and a high-resolution balloon sounding system at Shigaraki, Japan during October and November 1986. The observations were designed to examine the applicability of and the spectral amplitude limits implied by the linear saturation theory for gravity waves, to infer the dominant vertical scales of the fluctuation spectra, and to examine the spectral variability in time and its response to changes in atmospheric stability.

Our observations yielded broad support for the view that the fluctuation spectra are due primarily to gravity wave motions, with individual waves and phase progressions conspicuous in the velocity and temperature fields. Consistent with previous studies of the frequency spectra of atmospheric motions, the dominant contributions to the total energy were found to occur at intrinsic frequencies near the inertial frequency. The dominant motions above the zonal jet were found to exhibit a preferential downward phase progression and a clockwise rotation of the velocity vector with increasing height, indicative of an upward sense of propagation. Also observed was a tendency for wave propagation (and larger energies) in the meridional direction.

The main objective of the present study was to test the predictions of the saturated spectrum theory of Dewan and Good (1986) and Smith et al. (1987). The principal predictions of this theory are saturated amplitudes and spectral slopes of velocity and temperature

in vertical wavenumber given by Eqs. (5) and (7), with suitable modifications due to wave motions near the inertial frequency. Our observed mean velocity and normalized temperature spectra were found to be in excellent agreement with predicted spectral amplitudes and slopes, thus supporting the saturated spectrum theory and indicating consistency of the fluctuating velocity and temperature fields with the gravity wave dispersion relation. There was also general consistency with the theory of the spectra determined from individual velocity and temperature profiles. Agreement with the saturation theory was particularly good in the stratosphere where we anticipate that the motion spectrum is less influenced by other processes like convection.

Another objective of this study was to obtain an estimate of the dominant vertical scale of the motion spectrum. This was done using the area-preserving spectra and resulted in estimates of ~2.5 and 3 km from the velocity and temperature data, respectively. These support the findings of Fritts and Chou (1987), are comparable to the dominant vertical scales observed in the velocity and temperature data, and provide additional evidence for a consistent dynamical interpretation of the motion field. Also found was consistency of the area-preserving spectra of velocity and normalized temperature in time. This revealed variations in the total energy and of the dominant vertical wavelength on time scales of a few hours to days. Variations in the area-preserving spectra of temperature were seen to be consistent with those observed for velocity.

Finally, our comparison of the height profiles of mean variance of velocity and normalized temperature with N^2 variations revealed qualitative agreement. The agreement was particularly good for the normalized temperature variance and less complete for the velocity variance. In both cases, there was evidence of a relative enhancement in the variance in regions of increasing N^2, suggesting that such regions may be associated with an enhancement of saturated wave amplitudes.

Acknowledgments. Support for this work was provided in part by the Division of Atmospheric Sciences of the National Science Foundation under grant ATM-8404017 and by the Air Force Office of Scientific Research (AFSC) under contract F49620-87-C-0024. Additional support was provided by the Radio Atmospheric Science Center of Kyoto University, Kyoto, Japan, which operates the MU Radar. The authors are indebted to T. E. VanZandt and two reviewers for many useful comments on the manuscript.

REFERENCES

Balsley, B. B., and D. A. Carter, 1982: The spectrum of atmospheric velocity fluctuations at 8 and 86 km. *Geophys. Res. Lett.*, **9**, 465–468.

——, and R. Garello, 1985: The kinetic energy density in the troposphere, stratosphere and mesosphere: A preliminary study using the Poker Flat radar in Alaska. *Radio Sci.*, **20**, 1355–1362.

Desaubies, Y. J. F., 1976: Analytical representation of internal wave spectra. *J. Phys. Oceanogr.*, **6**, 976–981.

Dewan, E. M., and R. E. Good, 1986: Saturation and the "universal" spectrum for vertical profiles of horizontal scalar winds in the atmosphere. *J. Geophys. Res.*, **91**, 2742–2748.

——, N. Grossbard, A. F. Quesada and R. E. Good, 1984: Spectral analysis of 10 m resolution scalar velocity profiles in the stratosphere. *Geophys. Res. Lett.*, **11**, 80–83. Correction, **11**, 624.

Dong, B., and K. C. Yeh, 1988: Resonant and nonresonant wave-wave interactions in an isothermal atmosphere. *J. Geophys. Res.*, in press.

Dunkerton, T. J., 1982: Stochastic parameterization of gravity wave stresses. *J. Atmos. Sci.*, **39**, 1711–1725.

Endlich, R. M., R. C. Singleton and J. W. Kaufman, 1969: Spectral analysis of detailed vertical wind speed profiles. *J. Atmos. Sci.*, **26**, 1030–1041.

Fritts, D. C., 1984: Gravity wave saturation in the middle atmosphere: A review of theory and observations. *Rev. Geophys. Space Phys.*, **22**, 275–308.

——, and T. J. Dunkerton, 1985: Fluxes of heat and constituents due to convectively unstable gravity waves. *J. Atmos. Sci.*, **42**, 549–556.

——, and P. K. Rastogi, 1985: Convective and dynamical instabilities due to gravity wave motions in the lower and middle atmosphere: Theory and observations. *Radio Sci.*, **20**, 1247–1277.

——, and H.-G. Chou, 1987: An investigation of the vertical wavenumber and frequency spectra of gravity wave motions in the lower stratosphere. *J. Atmos. Sci.*, **44**, 3523–3532.

——, and T. E. VanZandt, 1987: The effects of Doppler shifting on the frequency spectra of atmospheric gravity waves. *J. Geophys. Res.*, **92**, 9723–9732.

——, and R. A. Vincent, 1987: Mesospheric momentum flux studies at Adelaide, Australia: Observations and a gravity wave/tidal interaction model. *J. Atmos. Sci.*, **44**, 605–619.

Fukao, S., K. Aoki, K. Wakasugi, T. Tsuda, S. Kato and D. A. Fleisch, 1981: Some further results on the lower stratospheric winds and waves over Jicamarca. *J. Atmos. Terr. Phys.*, **43**, 649–661.

——, T. Sato, T. Tsuda, S. Kato, K. Wakasugi and T. Makihira, 1985a: The MU radar with an active phased array system 1. Antenna and power amplifiers. *Radio Sci.*, **20**, 1155–1168.

——, T. Tsuda, T. Sato, S. Kato, K. Wakasugi and T. Makihira, 1985b: The MU radar with an active phased array system 2. In-house equipment. *Radio Sci.*, **20**, 1169–1176.

——, T. Sato, T. Tsuda, S. Kato, M. Inaba and I. Kimura, 1988: A systematic error in MST/ST radar measurement induced due to finite range volume effect, 1. Observational results. *Radio Sci.*, **23**, 59–73.

Garcia, R. R., and S. Solomon, 1985: The effect of breaking gravity waves on the dynamical and chemical composition of the mesosphere and lower thermosphere. *J. Geophys. Res.*, **90**, 3850–3868.

Hines, C. O., 1988: The generation of turbulence by atmospheric gravity waves. *J. Atmos. Sci.*, **45**, 1269–1278.

Hodges, R. R., Jr., 1967: Generation of turbulence in the upper atmosphere by internal gravity waves. *J. Geophys. Res.*, **72**, 3455–3458.

Holton, J. R., 1982: The role of gravity wave-induced drag and diffusion in the momentum budget of the mesosphere. *J. Atmos. Sci.*, **39**, 791–799.

Kato, S., T. Ogawa, T. Tsuda, T. Sato, I. Kimura and S. Fukao, 1984: The middle and upper atmosphere radar: First results using a partial system. *Radio Sci.*, **19**, 1475–1484.

Larsen, M. F., R. F. Woodman, T. Sato and M. K. Davis, 1986: Power spectra of oblique velocities in the troposphere and lower stratosphere observed at Arecibo, Puerto Rico. *J. Atmos. Sci.*, **43**, 2230–2240.

Lilly, D. K., D. E. Waco and S. I. Adelfang, 1974: Stratospheric mixing estimated from high-altitude turbulence measurements. *J. Appl. Meteor.*, **13**, 488–493.

Lindzen, R. S., 1981: Turbulence and stress owing to gravity wave and tidal breakdown. *J. Geophys. Res.*, **86**, 9707–9714.

Mantis, H. T., 1963: The structure of winds of the upper troposphere at mesoscale. *J. Atmos. Sci.*, **20**, 94–106.
——, and T. J. Pepin, 1971: Vertical temperature structure of the free atmosphere at mesoscale. *J. Geophys. Res.*, **76**, 8621–8628.
Meek, C. E., I. M. Reid and A. H. Manson, 1985: Observations of mesospheric wind velocities. II. Cross sections of power spectral density for 48–8 h, 8–1 h, 1 h–10 min over 60–110 km for 1981. *Radio Sci.*, **20**, 1383–1402.
Miyahara, S., Y. Hayashi and J. D. Mahlman, 1986: Interactions between gravity waves and the planetary scale flow simulated by the GFDL "SKYHI" general circulation model. *J. Atmos. Sci.*, **43**, 1844–1861.
Nastrom, G. D., and K. S. Gage, 1985: A climatology of aircraft wavenumber spectra observed by commercial aircraft. *J. Atmos. Sci.*, **42**, 950–960.
Palmer, T. N., G. J. Shutts and R. Swinbank, 1986: Alleviation of a systematic westerly bias in general circulation and numerical weather prediction models through an orographic gravity wave drag parameterization. *Quart. J. Roy. Meteor. Soc.*, **112**, 1001–1040.
Philbrick, C. R., K. U. Grossman, R. Hennig, G. Lange, D. Krankowsky, D. Offermann, F. J. Schmidlin, and U. von Zahn, 1983: Vertical density and temperature structure over Northern Europe. *Adv. Space. Res.*, **2**, 121–124.
Reid, I. M., and R. A. Vincent, 1987: Measurements of mesospheric gravity wave momentum fluxes and mean flow accelerations at Adelaide, Australia. *J. Atmos. Terr. Phys.*, **49**, 443–460.
Scheffler, A. O., and C. H. Liu, 1985: On observation of gravity wave spectra in the atmosphere by using MST radar. *Radio Sci.*, **20**, 1309–1322.
Schoeberl, M. R., D. F. Strobel and J. P. Apruzese, 1983: A numerical model of gravity wave breaking and stress in the mesosphere. *J. Geophys. Res.*, **88**, 5249–5259.
Smith, S. A., D. C. Fritts and T. E. VanZandt, 1985: Comparison of mesospheric wind spectra with a gravity wave model. *Radio Sci.*, **20**, 1331–1338.
——, —— and ——, 1987: Evidence of a saturation spectrum of atmospheric gravity waves. *J. Atmos. Sci.*, **44**, 1404–1410.
Strobel, D. F., J. P. Apruzese and M. R. Schoeberl, 1985: Energy balance constraints on gravity wave induced eddy diffusion in the mesosphere and lower thermosphere. *J. Geophys. Res.*, **90**, 13 067–13 072.
——, M. E. Summers, R. M. Bevilacqua, M. T. DeLand and M. Allen, 1987: Vertical constituent transport in the mesosphere. *J. Geophys. Res.*, in press.
Tanaka, H., 1986: A slowly varying model of the lower stratospheric zonal wind minimum induced by mesoscale mountain wave breakdown. *J. Atmos. Sci.*, **43**, 1881–1892.
Thomas, R. J., C. A. Barth and S. Solomon, 1984: Seasonal variations of ozone in the upper mesosphere and gravity waves. *Geophys. Res. Lett.*, **7**, 673–676.
VanZandt, T. E., 1982: A universal spectrum of buoyancy waves in the atmosphere. *Geophys. Res. Lett.*, **9**, 575–578.
——, and D. C. Fritts, 1988: A theory of enhanced saturation of the gravity wave spectrum due to changes in atmospheric stability. *Pure Appl. Geophys.*, in press.
Vincent, R. A., 1984: Gravity wave motions in the mesosphere. *J. Atmos. Terr. Phys.*, **46**, 119–128.
——, and I. M. Reid, 1983: HF Doppler measurements of mesospheric momentum fluxes. *J. Atmos. Sci.*, **40**, 1321–1333.
——, and D. C. Fritts, 1987: A morphology of gravity waves in the mesosphere and lower thermosphere over Adelaide, Australia. *J. Atmos. Sci.*, **44**, 748–760.
Yamanaka, M. D., and H. Tanaka, 1985: Hierarchical structure of stratospheric wind fluctuations. *Handbook for MAP*, **18**, 232–236.